

Supporting Information for

3D Flexible and Robust HAPs/PVA Separator Prepared by Freezing-Drying Method for Safe Lithium Metal Batteries

Wei Wang^{†,‡}, Yongchun Kan^{†,}, Can Liao[†], Kim Meow Liew[‡], Zonghai Chen[§], Lei Song[†],
and Yuan Hu^{†,*}*

[†] State Key Laboratory of Fire Science, University of Science and Technology of China,
96 Jinzhai Road, Hefei, Anhui 230026, People's Republic of China

*E-mail address: yuanhu@ustc.edu.cn (Y. Hu); yckan@ustc.edu.cn (Y. C. Kan)

[‡] Department of Architecture and Civil Engineering, City University of Hong Kong,
Tat Chee Avenue, Kowloon, Hong Kong

[§] Chemical Sciences and Engineering Division, Argonne National Laboratory, Argonne,
IL 60439, USA

Methods

Fabrication of electrolyte and electrodes.

Lithium bis borate (LiBOB), Lithium tablets with a scale of 15.4*0.45 mm, aluminum foils and all solvents (PC, NMP, Suzhou Duoduo Agents Co. Ltd) were lithium battery grade and used without any purification. Carbon black, LiFePO₄ and PVdF are provided by Saibo Agents Co. Ltd.

The cathode electrodes were fabricated by first well mixing the active materials of LiFePO₄ (no surface treatment), polyvinylidene difluoride (PVdF) and acetylene black (AB) in N-methylpyrrolidone with weight ratios of 80:10:10 (LiFePO₄: PVdF: AB).

The resultant slurry was cast on the Al foil (20mm thickness) using a 100 um doctor blade. The above electrodes were dried at 120 °C under vacuum for 12 h. The active material mass loading was 1-1.2 mg cm⁻² with a thickness of ~10-15 um, unless otherwise mentioned.

3D HAPs/PVA membranes preparation.

HAP nanorods were synthesized according to the hydrothermal method. Ca(NO₃)₂ 4H₂O, NH₄H₂PO₄ and NH₄OH (Sinopharm Chemical Reagent Co. Ltd. Analytically pure) were used without any purification. The mole ratio of Ca(NO₃)₂ 4H₂O, NH₄H₂PO₄ were was controlled by near 1.2. The above salts were completely dissolved in deionized water with a concentration of 0.4 mol L⁻¹. pH value of the resultant solution was adjusted to 9-10 by using NH₄OH. Then, the solution was transferred to Teflon cans and maintained at 170 °C for 15h. The obtained slurry was washed by deionized water until with a pH value of 7, and then dried at 80 °C overnight. The dried HAP

nanorods were obtained for further use. In the case of HAPs10%/PVA membrane with the mass ratio of 1:9: 1 g of HAP nanorods was dispersed in deionized water by constant stirring and sonication procedure for 2 h. Then, 9g of PVA was added into the above suspension by mechanical stirring and heating at 90 °C. Until the complete dissolution of PVA, the homogeneous white solution was cooled to room temperature (near 25 °C). The resultant HAPs/PVA (1/9) solution was cast on glass plate by using automatic coating machine. The thickness parameter was set at 200 μm . The glass plate coated with HAPs/PVA (1/9) solution was immersed into a coagulation bath containing 100% ethanol for 7 h. The coating temperature was controlled at 25 °C. After the immersion process, HAPs/PVA (1/9) membrane filled with ethanol was transferred to -60 °C under low pressure (1 pa) for 12 h in order to completely remove the ethanol. Then, the white membrane with high porosity was obtained and marked as HAPs10%/PVA. For the same rule, other separators with different mass ratio were also prepared by the same method and marked as PVA, HAPs1%/PVA, HAPs5%/PVA and HAPs20%/PVA. For comparison, PVA and HAPs10%/PVA membranes prepared at room temperature were also prepared. In a simple process, PVA or HAPs10%/PVA membrane filled with ethanol was kept at room temperature (25 °C) until the complete evaporation of ethanol. The resultant white membranes were obtained for further use.

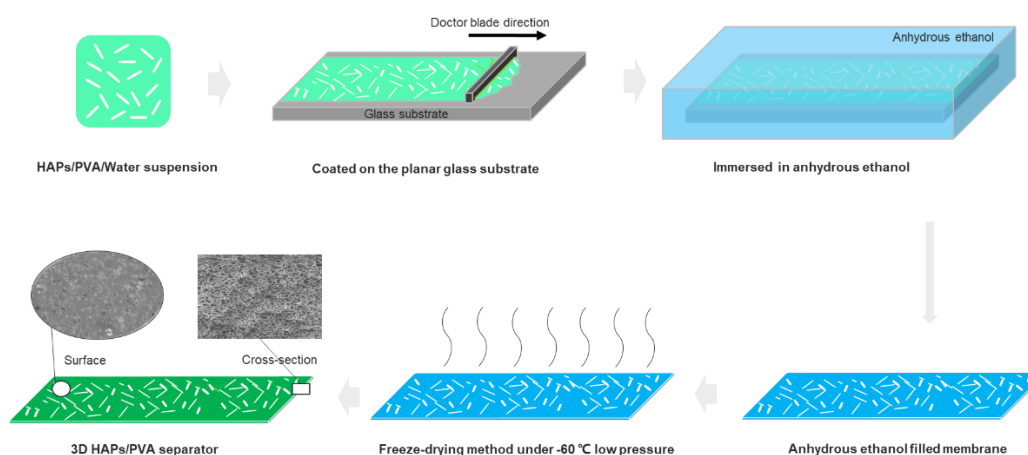


Figure S1. Schematic diagram of preparation procedure of 3D HAPs/PVA separator.

Material characterizations.

X-ray diffraction (XRD) measurements of HAP nanorods were performed on a Japan Rigaku D = Max-Ra rotating anode X-ray diffractometer equipped with a Cu–K α tube and Ni filter ($\lambda = 0.1542$ nm). Transmission electron microscopy (TEM) images of HAP nanorods were obtained on a transmission electron microscope (Hitachi model H-800). The morphologies of separators coated with a gold layer in advance were observed using field emission scanning electron microscopy (FESEM; AMRAY1000B, Beijing R&D Center of the Chinese Academy of sciences, China). The thermos-gravimetric analysis (TGA) of HAP nanorods and separators was carried out on a TGA-Q5000 apparatus (TA Co., USA) from 50 to 700 °C at a heating rate of 20 °C min⁻¹. The weight of all samples was maintained within 3-5 mg in an open platinum pan. The tensile strength and elongation at break of separators were measured according to the Chinese standard method (GB 13022-91) with a WD-20D electronic universal testing instrument (Changchun Intelligent Instrument Co., Ltd., China) at a crosshead speed of 50 mm min⁻¹. The dimensions of specimens are 20 mm \times 4 mm \times specified thickness (Lo \times b \times d), the specified thickness is measured by caliper (Mitutoyo made in Japan,

Range: 0-25 mm, Accuracy: 0.0001 mm). The test of mechanical properties was performed for at least three times. Thermal stability of the separator was examined by a differential scanning calorimeter (Diamond DSC, PerkinElmer) ranging from 50 to 200 °C at 10 min⁻¹ under N₂ atmosphere. A micro-combustion calorimeter (MCC, GOVMARK) was used to evaluate the combustion properties of the separators according to ASTM D 7309-07. Samples with 4-6 mg were heated in nitrogen atmosphere at a constant heating rate 1 °C s⁻¹ from room temperature to 700 °C. The decomposition products were mixed with 20 mL/min oxygen and then burned in the combustion furnace at 900 °C. The thermal shrinkage properties of Celgard separator, control PVA and PVA/HAP separators were placed on oven and heated at 100, 120, 140, 160, and 180 °C for 0.5 h, respectively. The Young's modulus of separators is evaluated by the Atomic Force Microscope (Bruker, Demension Icon), the silicon probe of RTESP-525 was chosen.

The porosities of Celgard separator and PVA-based separators were measured using n-butanol absorption method. The mass of the separators was measured before and after immersion in n-butanol for 3h. The porosities of separators were calculated by the following equation:

$$\text{Porosity (\%)} = \frac{M_a - M_b}{\rho V} \times 100\%$$

where M_b and M_a are the weight of the separators before and after soaking in n-butanol for 3h, respectively; before calculating, the excess electrolyte on the surface should be wiped clean; ρ is the density of n-butanol; V is the volume of specimen. Wettability was evaluated by measuring the contact angle with a sessile drop method using a SL200B

Contact Angle System (Solon Tech. Co., Ltd., China). The electrolyte droplet volume was 5 μL . The measurements were carried out under ambient conditions (25 $^{\circ}\text{C}$).

The electrolyte uptake was obtained by measuring the weight of separators before and after liquid electrolyte (1 M $\text{LiPF}_6/\text{EC}:\text{DMC}$ 1:1 v/v) soaking for 2 h and then calculated using following equation:

$$\text{Electrolyte Uptake (\%)} = \frac{W_a - W_b}{W_b} \times 100\%$$

where W_b and W_a are the weights of separators before and after soaking in the liquid electrolyte, respectively.

To examine the thermal stability, the thermal shrinkage ratio was calculated according to the following equation:

$$\text{Thermal Shrinkage (\%)} = \frac{A_a - A_b}{A_a} \times 100\%$$

Where A_a and A_b are the areas of the separator before and after thermal treatment at various temperatures for 0.5 h.

Electrochemical Measurements

For measurements of electrochemical performance, the liquid electrolyte of 1 M LiPF_6 in EC/DMC (1/1, v/v) was employed. The electrochemical stability window of the separators was measured by a linear sweep voltammetry (LSV) experiment performed on a working electrode of stainless-steel and a counter electrode of lithium metal at a scanning rate of 1.0 mV s^{-1} . The bulk impedance (R_b) of separators was estimated by the electrochemical impedance spectroscopy (EIS) (Shanghai Chenhua 670 electrochemical workstation). The electrolyte-soaked separators were fabricated between two pieces of stainless steel (SS) and the spectra was recorded over a frequency

range from 0.01 Hz to 1 MHz with the AC amplitude of 10 mV under open circuit potential condition at room temperature (25 °C). The ionic conductivity (σ) was calculated according to the following equation.

$$\sigma = \frac{d}{Rb \times A}$$

where d and A are the thickness and effective area of a membrane, respectively.

A half cell (2032-type coin) was assembled by sandwiching a separator between a LiFePO₄ cathode (LiFePO₄ /carbon black/PVDF 80/10/10 w/w/w) and a lithium metal anode, and then filling with the 80 μ l of the liquid electrolyte of 1 M LiPF₆ in EC/DMC (1:1, v/v) for the room temperature test and the liquid electrolyte of 0.8 M LiBOB in polar solvent of PC for the high temperature test. All assembly process of cells was carried out in an argon filled glove box (O₂ < 0.1 ppm, H₂O < 0.1 ppm). For the fair comparison, the cells using the Celgard separator (Celgard 2325) were assembled and tested under the same conditions. The charge/discharge rates were varied from 0.1 to 2 C under a voltage range between 2.8 and 4.2 V. The cells were cycled at a fixed charge/discharge rate at 0.2 C / 0.2 C (1C= 170 mA g⁻¹) for the first five cycles and then changed to 0.5 C/0.5 C for the following cycles at room temperature. The galvanostatic charge–discharge was performed in the voltage window of 2.8–4.2 V on a Land automatic battery tester (Wuhan, China). The high temperature cells were cycled at a fixed charge/discharge rate at 0.5 C/0.5 C under 120 °C.

Characterization of HAPs.

HAPs, as an environmentally friendly inorganic mineral and with high thermal and chemical stability, excellent electrical insulation and great fire resistance, can ensure the compositional and structural stability of separators during working procedure of lithium batteries at extreme conditions. Herein, HAPs are prepared with a purpose to build a microstructure with high porosity combined with PVA resin (hydrolysis: 99%). Attributing to the high abundance of functional groups such as hydroxyl groups, PVA and HAPs can thereby achieve a high affinity with each other and promising mechanical properties by substantial interfacial interactions, for instance, hydrogen bonds and van der Waals forces. In this work, HAPs possess structural scales with a diameter of 20 nm and a length of 100 nm (Figure S2c, d, Supporting Information). XRD pattern (Figure S2a, Supporting Information) is also confirmed the successful synthesise of HAP nanorods (JCPDS card: No. 24-0033). To evaluate the thermal stability of HAP nanorods, TGA curve (Figure S2b, Supporting Information) of HAPs is also provided, presenting the highly thermal stability of HAP nanorods with a mass loss of 3.5% at 800 °C.

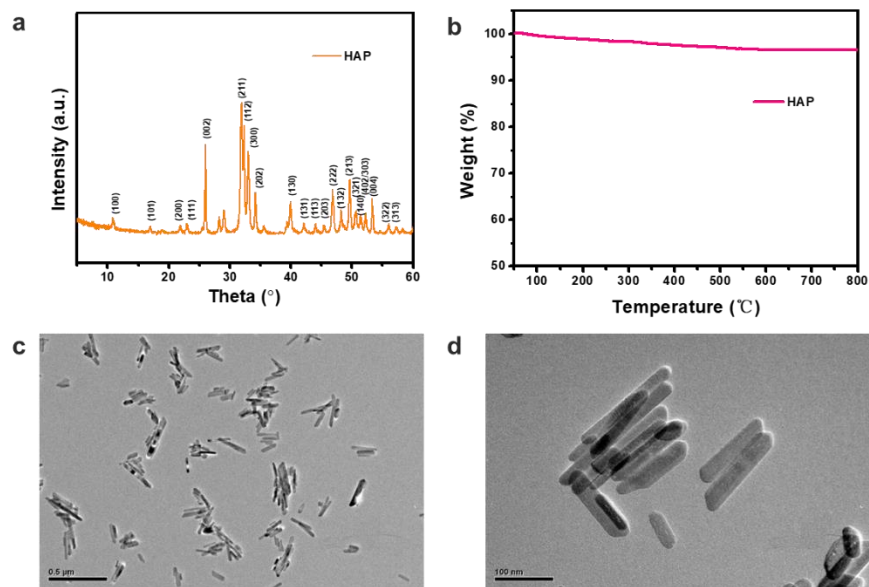


Figure S2. a) XRD pattern of HAP nanorods. b) TGA curve of HAP nanorods. c, d) TEM images of HAP nanorods under various magnification.

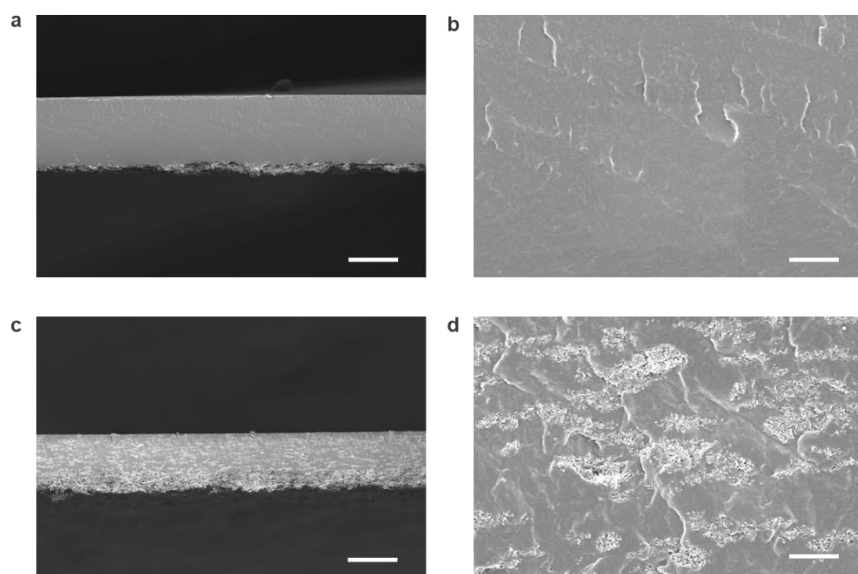


Figure S3. SEM images of cross-section of a, b) PVA membrane and c, d) HAPs10%/PVA membrane prepared at room temperature (25 °C) with the scale bar of 25 μm and 2 μm , respectively.

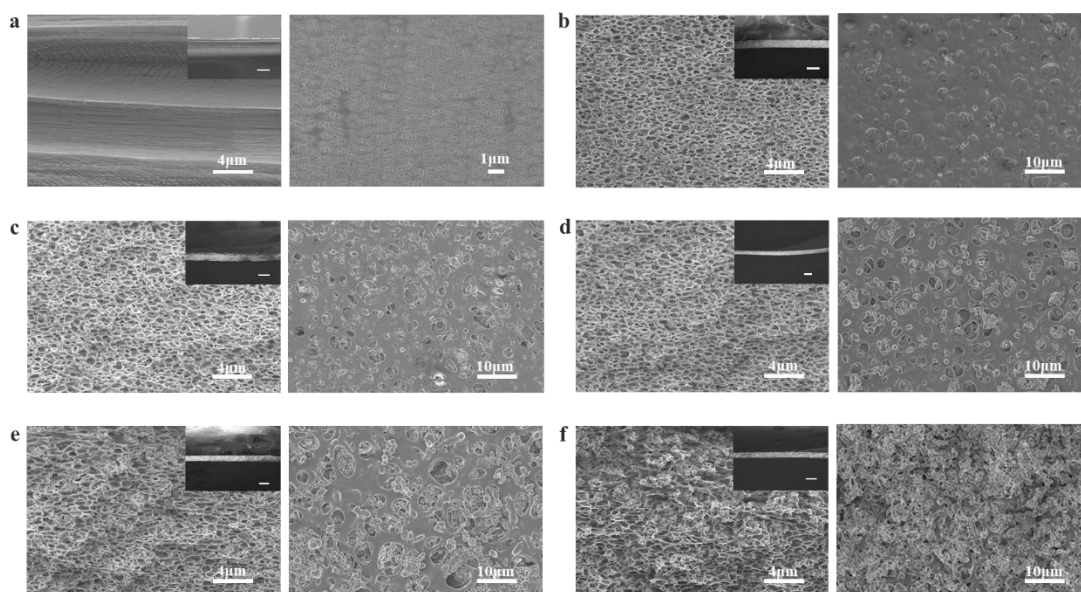


Figure S4. SEM images of cross-section (left) and the surface (right) of a) Celgard membrane, b) PVA membrane, c) HAPs1%/PVA membrane, d) HAPs5%/PVA membrane, e) HAPs10%/PVA membrane, and f) HAPs20%/PVA membrane prepared at a low temperature (~ 60 °C). The insert images are the cross-section under low magnification, the insert scale bar is near 50 μm . The thickness of control PVA separator and PVA/HAP separators are controlled at near 40-50 μm by adjusting the height parameter of doctor blade.

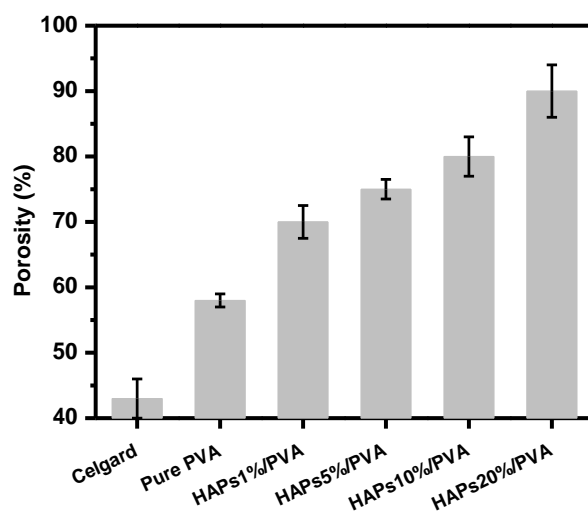


Figure S5. The porosity values of different separators. By calculating the weight of the separators before and after soaking in n-butanol, porosity can be obtained.

Wettability and Contact angle test.

In the case of nonpolar polyolefin-based separators such as PE and PP, owing to their intrinsically hydrophobic feature and low surface energy, these separators usually possess poor affinity with conventional polar liquid electrolytes, which greatly limits the electrochemical performance and brings about additional issues to battery fabrication procedures. On the contrary, PVA possesses large amount of hydrogen groups, which can achieve a better affinity with polar liquid electrolytes. Electrolyte uptake data is presented in Figure S6b. The electrolyte uptake results reveal that hybridizing with HAP, HAPs10%/PVA separator achieves a much higher electrolyte uptake (275%) compared with commercial Celgard separator (83%) and PVA separator (102%), indicating a good affinity with liquid electrolyte. Interestingly, in the case of the high loading (20 wt.%), the electrolyte uptake has a decrease trend, the proposal explanation is revealed: the higher loading of HAP could lead to a larger porosity and surface holes (Figure S4 and Figure S5, Supporting Information) but also lead to the weak absorption force to liquid electrolytes, which thereby restricting the behavior of electrolyte uptake. Additionally, the diffusion behavior of HAPs10%/PVA separators have also been evaluated by the dipping test shown in Figure S6a. The electrolyte diffusion height of PVA and HAPs10%/PVA separators are respectively 9 and 21 mm, showing a much higher electrolyte compatibility than that of Celgard separator (< 2 mm). The above results proved that HAPs/PVA has superior electrolyte wettability than PVA and Celgard separators. Contact angle test was employed to further investigate the electrolyte wettability of separators, the corresponding results are provided in Figure

S7 and Figure S8. PVA-based separators achieve a much lower contact angle ($< 20^\circ$) compared with that of Celgard separator ($\sim 70^\circ$) after dropping the liquid electrolyte on their surfaces for 100 s. Moreover, as the addition up to at least 10 wt.%, the contact angles shift to $\sim 0^\circ$ in a very short time (< 3 s). By reason of this, the ion conductivities (Figure S9) and impedance (Figure S10) of the HAPs-based separators also perform more advanced than those of Celgard and PVA separators. The ion conductivity values of HAPs-based separators with a loading of > 10 wt. % can reach up to $\sim 2.0 \text{ mS cm}^{-1}$, which are almost an order of magnitude more than those of PVA (0.22 mS cm^{-1}) and Celgard separator (0.41 mS cm^{-1}). The high electrolyte affinities of HAPs/PVA are mainly ascribed to strongly interfacial forces among polar liquid electrolytes, hydrogen bonds from PVA and HAPs the highly porous structure as well as the highly electrolyte affinity with HAPs.

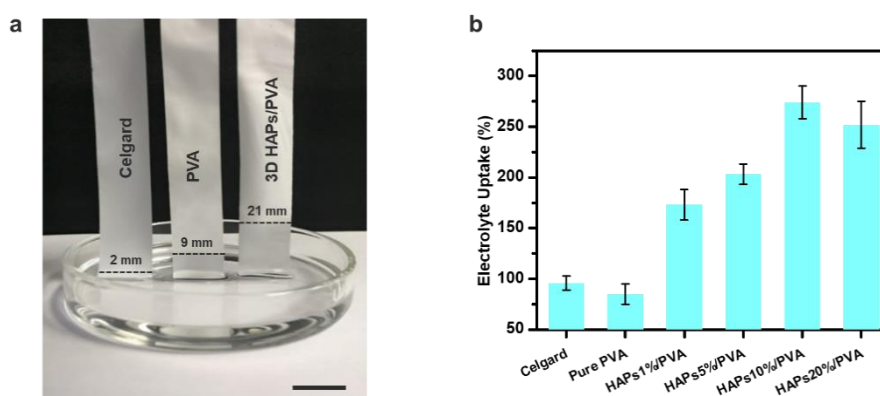


Figure S6. a) Photograph of electrolyte immersion-height of Celgard separator, pure PVA separator and HAPs10%/PVA separator after immersion of 30 min. The insert scale bar represents 2 cm. b) The electrolyte uptake values of different separators. The electrolyte is 1 M LiPF₆/EC: DMC 1:1 v/v. The above tests were conducted at ambient temperature (25 °C).

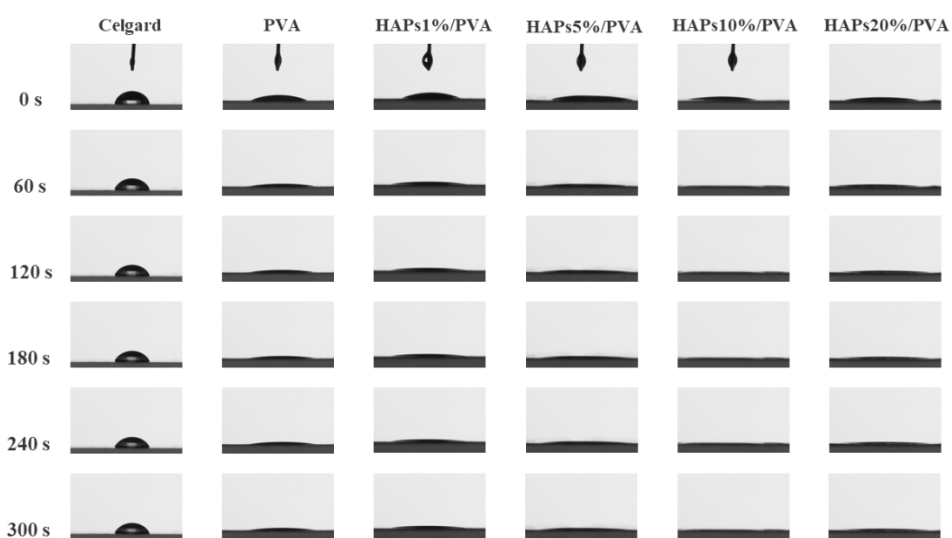


Figure S7. Contact Angle of Celgard separator, pristine PVA separator and HAPs/PVA separators as a function of time with electrolyte (1 M LiPF₆/EC: DMC 1:1 v/v). The operation temperature is near 25 °C.

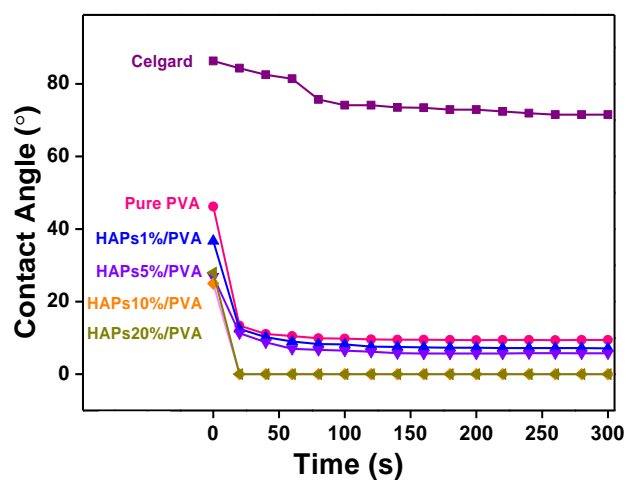


Figure S8. Contact angle of the Celgard separator, PVA separator and HAPs/PVA separators after dropping a liquid electrolyte (1 M LiPF₆/EC: DMC 1:1 v/v) for different times: from 0 min to 5 min, the interval is 20 s.

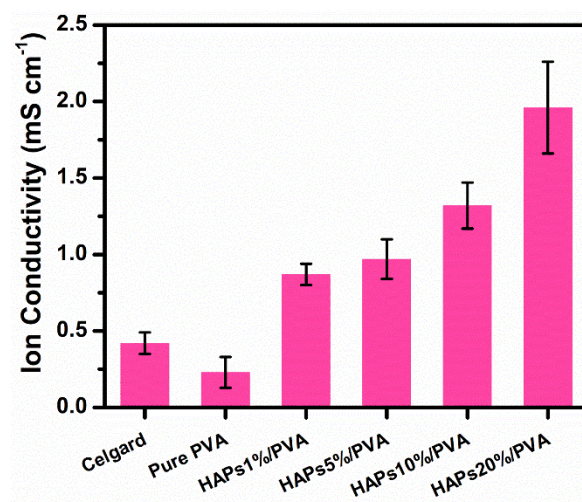


Figure S9. The ion conductivities of different separators.

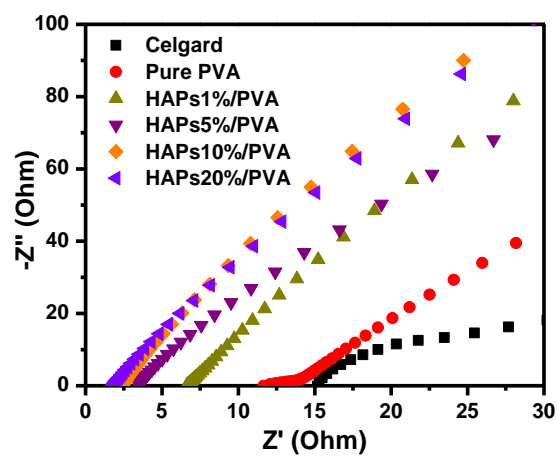


Figure S10. Nyquist plots of different separators by using a Steel|Electrolyte soaked Separators|Steel system. The spectra were recorded over a frequency range from 0.01 Hz to 1 MHz.

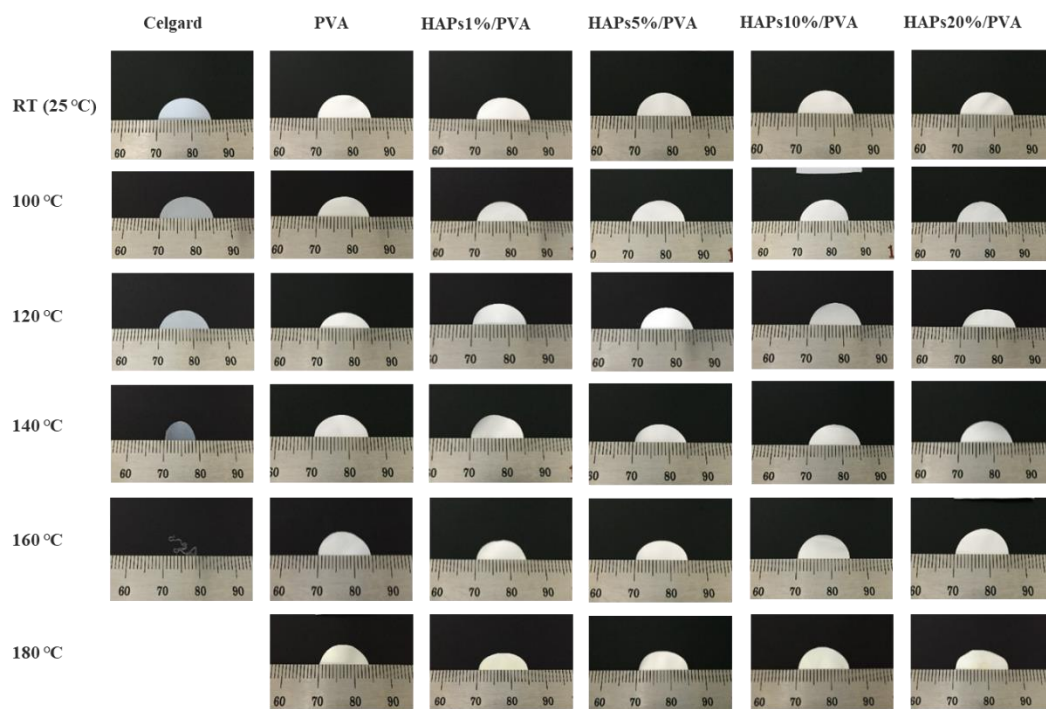


Figure S11. Thermal shrinkage photos selected after maintained in oven at a certain temperature for 0.5 h. The original diameter of separators is 16mm. After at high temperature, the diameter scales are measured by steel rule.

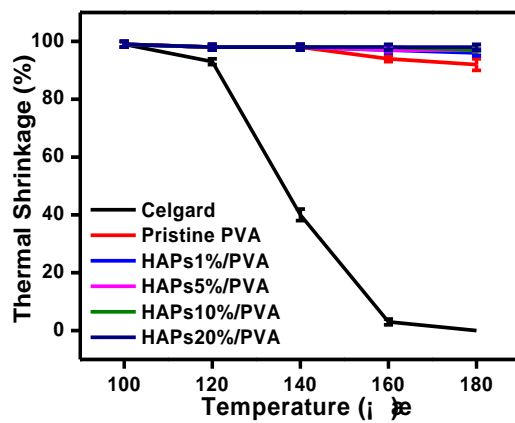


Figure S12. The thermal shrinkage area of Celgard separator, control PVA and HAPs/PVA separators were selected after with thermal treatment at 100, 120, 140, 160, and 180 °C for 0.5 h.

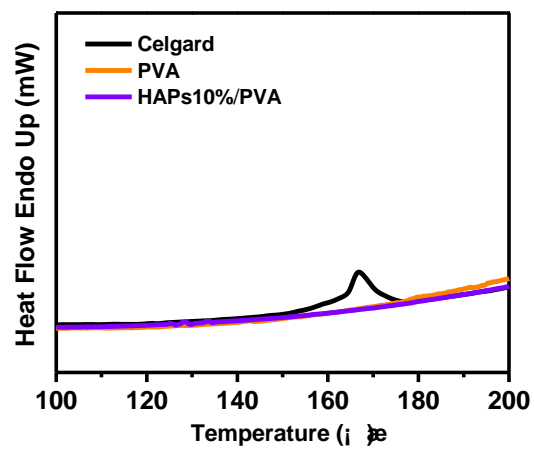


Figure S13. DSC curve of Celgard separator, pristine PVA separator and HAPs10%/PVA separator with a range of 100 - 200 °C.

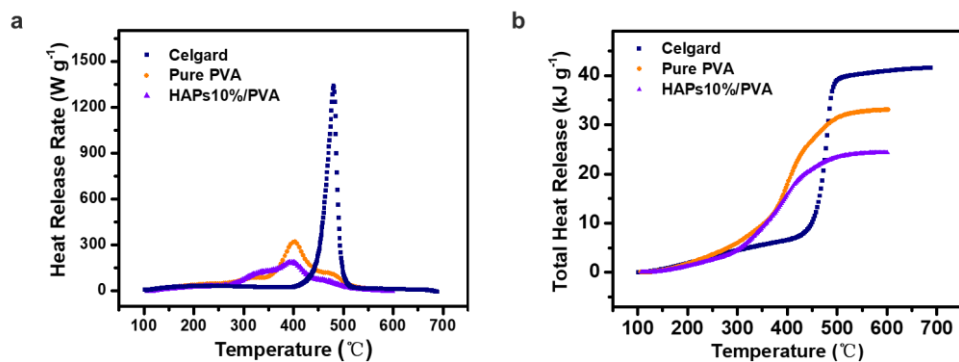


Figure S14. a) Heat release rate and b) total heat release of Celgard separator, pristine PVA separator and HAPs10%/PVA separator.

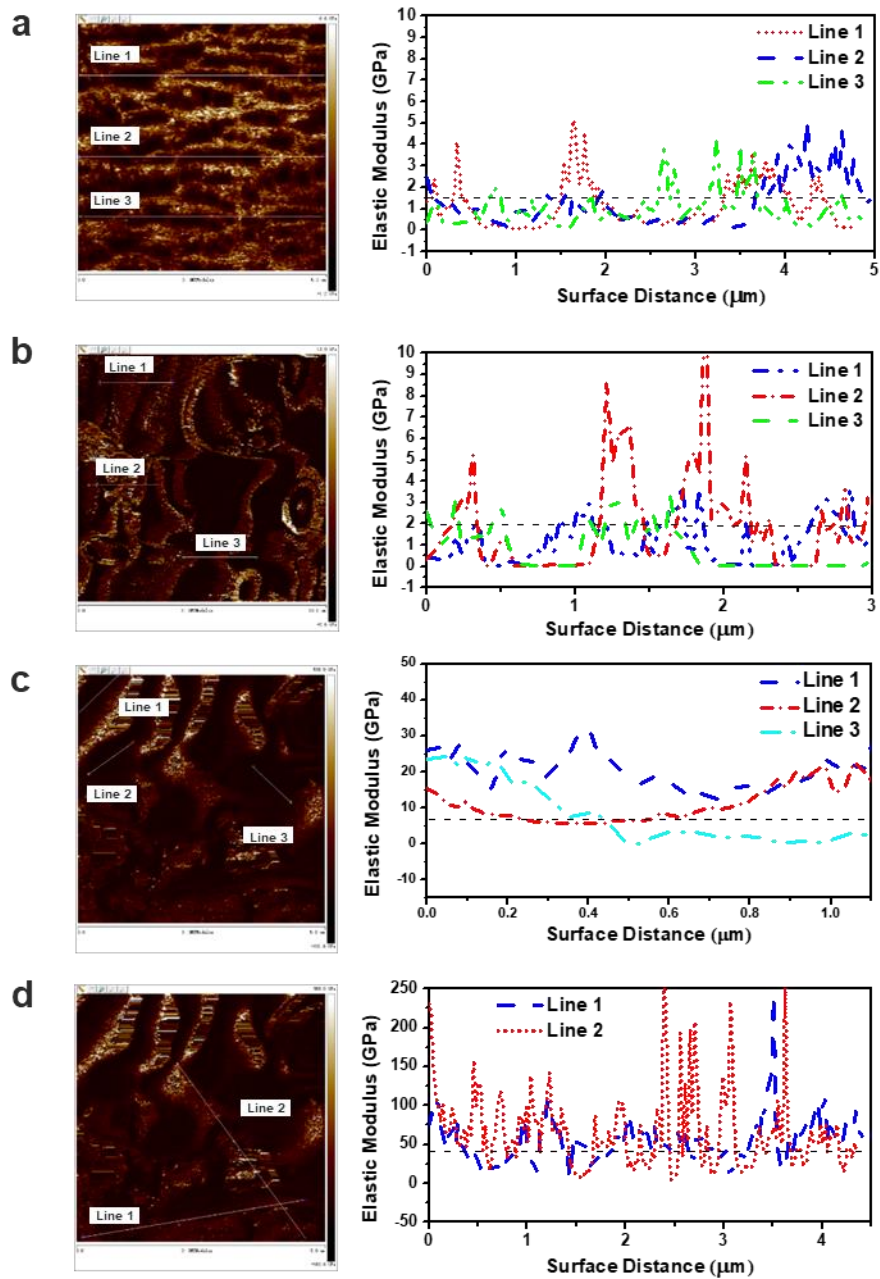


Figure S15. The Young's modulus mapping and corresponding partial modulus in detail of a) Celgard separator; b) pristine PVA separator; c) low modulus region and d) high modulus region of HAPs10%/PVA.

Table S1. Comparison of Young's modulus of the as-prepared 3D HAPs/PVA separator with those of separators or layers previously reported for lithium metal batteries.

| Separators/layers | Young's modulus (GPa) | Reference |
|--|--------------------------|-----------|
| (PEO/ANF) ₁₀₀ | ~5 | 1 |
| Artificial Li ₃ PO ₄ SEI layer | ~11 | 2 |
| BN-coated separator | Not provided. | 3 |
| ZrO ₂ /POSS multilayer-assembled PE separator | Not provided. | 4 |
| Artificial Cu ₃ N + SBR layer | ~0.81 | 5 |
| Novel silica Nanoparticle sandwiched separator | Not provided. | 6 |
| POSS-2PEG6K layer | Not provided. | 7 |
| PBO-NMs | ~20 | 8 |
| PVDF-HFP/Al ₂ O ₃ separator | ~0.5 | 9 |
| 3D HAPs/PVA separator | ~35 | This work |

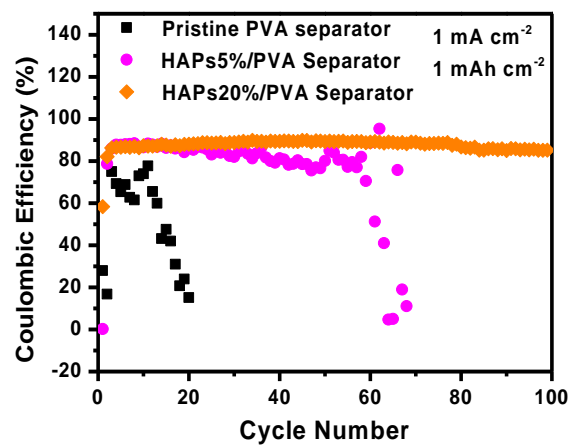


Figure S16. Coulombic efficiency obtained from Li|Cu cells using pristine Celgard separator, HAPs5%/PVA separator and HAPs20%/PVA separator at a current density of 1 mA cm^{-2} . The amount of Li deposited in each cycle is 1 mAh cm^{-2} .

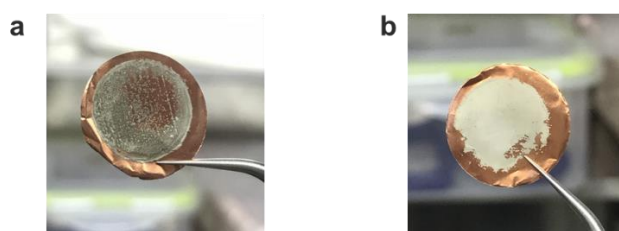


Figure S17. The camera digital photos of Li deposition after first deposition on bare Cu foil with a fixed amount of Li (1 mAh cm^{-2}). a) Celgard separator, b) the 3D HAPs/PVA separator.

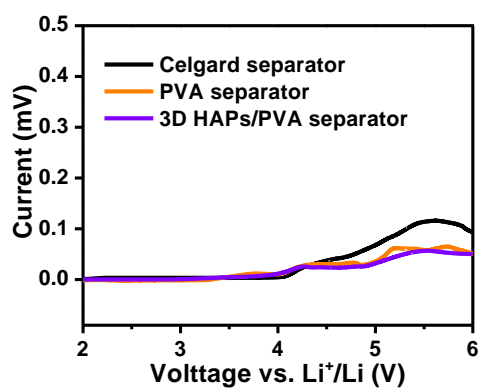


Figure S18. Linear sweep voltammetry of the Celgard separator, pristine PVA separator, and the 3D HAPs/PVA separator fabricated in Li|separator-liquid electrolyte|stainless steel cells at a scan rate of 1.0 mV s^{-1} .

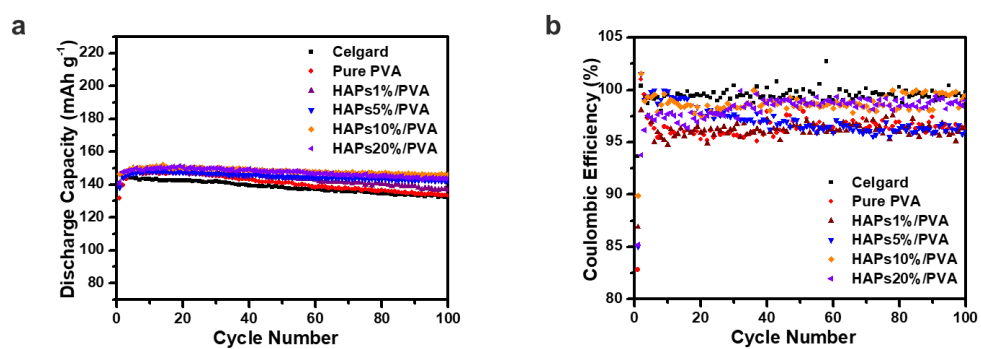


Figure S19. Electrochemical performances of Lithium metal batteries. a) Cycling performances and Coulombic efficiency of the LiFePO_4 |3D HAPs/PVA-liquid electrolyte|Li and LiFePO_4 |Celgard separator-liquid electrolyte|Li cells at C/5 for 100 cycles. ($1C=170 \text{ mA g}^{-1}$).

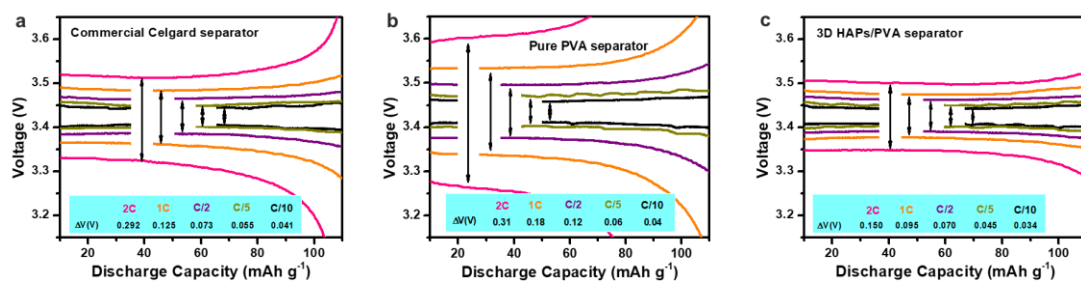


Figure S20. The polarization of the half-cells using a) Celgard separator and b) PVA separator and c) 3D HAPs/PVA separator at C/10, C/5, C/2, C and 2C, respectively. The insert data represents the voltage gaps at different current density.

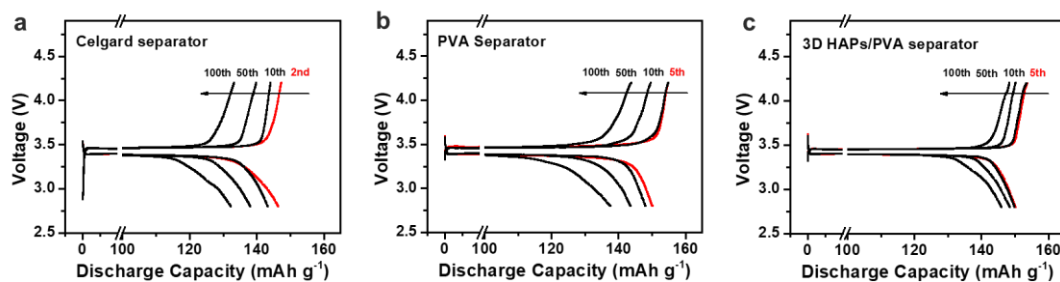


Figure S21. Charge-discharge voltage curves of the cells using c) the Celgard separator, d) control PVA separator and e) the 3D HAPs/PVA separator at a rate of $C/5$. The curves of 2nd or 5th, 10th, 50th and 100th cycles are shown. In the case of PVA-based separators, the charge-discharge capacity has an increasing trend before the first 5 cycles. The capacity in 5th is chosen for the first one.

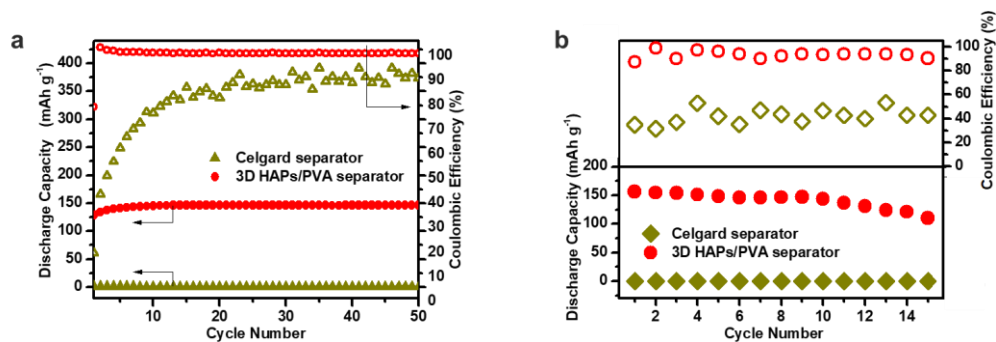


Figure S22. The cycling performance of LiFePO₄/Li half cells with the Celgard separator and the 3D HAPs/PVA separator and the electrolyte of 0.8 M LiBOB/propylene carbonate at a rate of C/2. The conducted temperatures are a) 25 °C and b) 110 °C, respectively.

Reference

1. S.-O. Tung, S. Ho, M. Yang, R. Zhang and N. A. Kotov, *Nat. Commun.*, 2015, **6**, 6152.
2. N. W. Li, Y. X. Yin, C. P. Yang and Y. G. Guo, *Adv. Mater.*, 2016, **28**, 1853-1858.
3. W. Luo, L. Zhou, K. Fu, Z. Yang, J. Wan, M. Manno, Y. Yao, H. Zhu, B. Yang and L. Hu, *Nano lett.*, 2015, **15**, 6149-6154.
4. M. Chi, L. Shi, Z. Wang, J. Zhu, X. Mao, Y. Zhao, M. Zhang, L. Sun and S. Yuan, *Nano energy*, 2016, **28**, 1-11.
5. Y. Liu, D. Lin, P. Y. Yuen, K. Liu, J. Xie, R. H. Dauskardt and Y. Cui, *Adv. Mater.*, 2017, **29**, 1605531.
6. K. Liu, D. Zhuo, H.-W. Lee, W. Liu, D. Lin, Y. Lu and Y. Cui, *Adv. Mater.*, 2016, **29**.
7. Q. Pan, D. M. Smith, H. Qi, S. Wang and C. Y. Li, *Adv. Mater.*, 2015, **27**, 5995-6001.
8. X. Hao, J. Zhu, X. Jiang, H. Wu, J. Qiao, W. Sun, Z. Wang and K. Sun, *Nano lett.*, 2016, **16**, 2981-2987.
9. Z. Tu, Y. Kambe, Y. Lu and L. A. Archer, *Adv. Energy Mater.*, 2013.